Study of atmospheric muons using a cosmic ray telescope

2013 J. Phys. G: Nucl. Part. Phys. 40 025202

(http://iopscience.iop.org/0954-3899/40/2/025202)

IOP Publishing Journal of Physics G: Nuclear and Particle Physics

J. Phys. G: Nucl. Part. Phys. **40** (2013) 025202 (9pp) doi:10.1088/0954-3899/40/2/025202

Study of atmospheric muons using a cosmic ray telescope

S Abdollahi[1,2], M Bahmanabadi[1] and D Purmohammad[2]

[1] Department of Physics, Sharif University of Technology, PO Box 11155-9161, Tehran, Iran
[2] Science Faculty, Imam Khomeini International University, Qazvin, Iran

E-mail: abdollahi.soheila@gmail.com

Received 26 April 2012
Published 16 January 2013
Online at stacks.iop.org/JPhysG/40/025202

Abstract

The charge ratio of cosmic muons holds important information for both the atmospheric neutrino anomaly and hadronic interaction models. In this paper we measured the muon charge ratio ($R_\mu = N_{\mu^+}/N_{\mu^-}$) in the cosmic ray flux in the momenta range 0.76–1.60 GeV/c by using a cosmic ray telescope. The delayed coincidence method is used based on the reduced mean lifetime of negative muons due to nuclear capture in matter. The systematic time-dependent effects of the muon charge ratio are considered by grouping the decay data into different time intervals. We compared the experimental data with the predictions of CORSIKA simulations using a high energy interaction model (QGSJET-II) and two low energy interaction models (UrQMD and GHEISHA) in the energy range 10^{11}–10^{16} eV for primary particles. In addition, by considering the muon flux in different zenithal and azimuthal angles, the muon angular distribution is obtained as $I(\theta) = I(0)\cos^n\theta$ with average $n = 1.91 \pm 0.07$. Dependence of the muon flux on the azimuth angle (the East–West effect) is also observed, due to the influence of the geomagnetic field in particular on low energy muons.

(Some figures may appear in colour only in the online journal)

1. Introduction

Primary cosmic rays are mainly protons, alpha particles and heavier ionized nuclei impinging upon the Earth's atmosphere. These primary cosmic rays induce a cascade of secondary particles which is called an extensive air shower (EAS). Generally the most common secondary particles are unstable charged particles (baryons and mesons) that decay into muons.

$$\pi^\pm \to \mu^\pm + \nu_\mu(\overline{\nu}_\mu) \qquad \sim 100\% \text{ (mean life time 26 ns)} \tag{1}$$

$$\kappa^\pm \to \mu^\pm + \nu_\mu(\overline{\nu}_\mu) \qquad \sim 63.5\% \text{ (mean life time 12 ns)} \tag{2}$$

Muons decay with a longer mean lifetime (2.2 μs) according to:

$$\mu^\pm \to \mathrm{e}^\pm + \nu_\mathrm{e}(\overline{\nu}_\mathrm{e}) + \overline{\nu}_\mu(\nu_\mu). \tag{3}$$

The muon charge ratio is a substantial quantity which reflects important features of hadronic meson production in cosmic ray collisions; it is also strongly related to the neutrino flux and provides relevant information for neutrinos physics [1, 2].

$$R_\mu (N_{\mu^+}/N_{\mu^-}) \approx R(N_{\nu_e}/N_{\overline{\nu}_e}) \tag{4}$$

where N_{μ^+} and N_{μ^-} are the number of positive and negative muons and N_{ν_e} and $N_{\overline{\nu}_e}$ show the number of electronic neutrinos and antineutrinos respectively.

So since neutrinos and antineutrinos interact with matter in different ways, the charge ratio also contains important information for evaluating neutrino detector responses. The measured value of the muon charge ratio, which varies empirically between values of about 1.10–1.30, is mainly due to the proton excess in primary cosmic rays as a small excess of positive pions in the collision process leads to a single shower with a value of $R_\mu (N_{\mu^+}/N_{\mu^-}) > 1$ [3].

A rough addition of the neutrino flavours involved in equations (1)–(3) leads to the ratio:

$$R_\nu = (N_{\nu_\mu} + N_{\overline{\nu}_\mu})/(N_{\nu_e} + N_{\overline{\nu}_e}) = 2. \tag{5}$$

However more detailed studies indicate an energy dependence of all the ratios. The ratio of muon neutrinos to electron neutrinos (R_ν) shows a strong dependence as the number of muons reaching sea-level before decaying increases. Hence at high energies the muon decay no longer contributes and R_ν is larger than 2.

The measured ratio of muon neutrinos to electron neutrinos by Super-Kamiokande and other experiments appears to be significantly less than the theoretical prediction—known as the atmospheric neutrino anomaly [4, 5]. Because the flux of electron neutrinos seems to agree with the expectation, this anomaly mainly results from a lack of muon neutrinos and has been interpreted to be due to flavour oscillation of $\nu_\mu \rightarrow \nu_\tau$ [6].

Several experimental techniques have been applied to measure the muon charge ratio. In most experiments, the separation of positive and negative particles is carried out through use of magnetic spectrometers. In very low momenta ranges, the use of spectrometers is not appropriate due to the large percentage of electrons present in secondary cosmic rays; different acceptances for positive and negative particles cause a large systematic error in the measurements of the muon charge ratio [7].

Another experimental procedure is the 'delayed coincidences method' based on the reduced mean lifetime of negative muons due to nuclear capture in matter. The study of muon flux at different azimuthal angles shows an asymmetry in muon angular distribution from East to West that can be attributed to the effect of the Earth's magnetic field which deflects the trajectories of charged secondary particles (the East–West effect) [8]. Also zenithal distribution of muon flux is obtained as a power function of $\cos\theta$.

In this paper, to determine the muon charge ratio and to study the muon angular distribution, we carried out a series of experiments using a cosmic ray telescope at Sharif University of Technology (SUT), Tehran and simulated EASs with CORSIKA [9] code (version 6.9) to compare the experimental data with simulated predictions. The statistics and precision of results reported in this paper are more accurate than our previous measurements [10, 11] and so in simulations we will compare the results of two different hadronic interaction models at low energy.

2. Method and experimental set-up

The cosmic ray telescope consists of two plastic scintillators ($30 \times 10 \times 1\,\mathrm{cm}^3$) spaced 1 m from each other. Photons are produced by passing particles through the scintillators and are sent to two photomultiplier tubes (PMT, 9813B with diameters of 5 cm) via plastic light guides.

Table 1. Mean lifetime and decay probability of negative muons in different media.

Medium	Mean lifetime (ns)	Decay probability (%)
Vacuum	2197.03 ± 0.04	100.00
Carbon	2026.3 ± 1.5	92.15
Oxygen	1795.4 ± 2	81.57
Aluminium	864.0 ± 1	39.05
Lead	75.4 ± 1	2.75

This telescope is a rotatable device around its vertical axis in different zenithal and azimuthal angles and is installed on the fourth floor of the Physics Department of SUT, Tehran (35°43′N, 51°20′E) 1200 m above sea-level corresponding to an average atmospheric depth of 890 gcm^{-2}. The fourth floor is under two concrete roofs which are equivalent to about 150 gcm^{-2}, so that the total mass above the telescope (in a vertical position) is about 1040 gcm^{-2}, i.e. near to atmospheric thickness at sea-level.

To determine the muon charge ratio, the telescope was set in a vertical position. We used the delayed coincidences method to take into account the different behaviour of positive and negative muons with the matter. Positive muons can only decay, while negative muons can be trapped in atomic orbit so that they may decay or be absorbed by atomic nuclei which reduces their mean lifetime. The probability of negative muon capture by atomic nuclei is proportional to Z^4 where Z is the atomic number of host atoms [12]. Thus the lifetime of negative muons decreases significantly for high Z atoms. Table 1 shows the mean life times and decay probabilities of negative muons in different media [13].

In compounds muon capture is caused by the nucleus with the larger muon capture rate, i.e. with a lower decay probability and larger atomic number. For instance, in a plastic scintillator (polyvinyl-toluol, $2 - \mathrm{CH_3C_6H_4CH} = \mathrm{CH_2}$ monomer) only the carbon capture is significant [7].

After passing through the top scintillator low energy muons may stop in the bottom scintillator and decay into electrons (positrons). The emitted electron will be detected if its pulse height is greater than the threshold value of the discriminator which is adjusted for the bottom scintillator.

As the incident muon hits both scintillators, the signals generated in the two PMTs are entered into an eight-channel fast discriminator (CAEN N413A), after amplifying by a fast amplifier ($\times 10$, CAEN N412). The discriminator thresholds are set to values of 50 and 23 mV for the signals of the top and the bottom scintillators respectively. In this way the outputs of the discriminator are connected to a logic unit (CAEN N405) with a gate width of 150 ns. Then the output of the logic unit is connected to the 'start' input of a time-to-amplitude converter (TAC, ORTEC 566) with a time range of 10 μs, by a 10 m delay cable. So a signal generated by the emitted electron of muon decay in the bottom scintillator, after passing through an amplifier ($\times 10$) and discriminator, is connected to the 'stop' input of the TAC. In this way the time interval between the signal of the stopped muon and detection of the emitted electron is measured. Finally the output of the TAC is sent to a multi-channel analyser (MCA) via an analogue-to-digital converter unit (ADC). Figure 1 shows the scheme of the electronics layout used to record the muon decay.

In addition, we ran a series of experiments using the coincidence method to further study the muon flux in different azimuthal and zenithal angles, the results of which will be discussed in the next section. In these experiments the muons which pass through both scintillators are considered. Thus the signal generated by the top PMT is sent to the 8-channel fast discriminator, with a threshold of 23 mV, after amplification by the fast amplifier. Then the output of the discriminator is connected to the 'start' input of the TAC. In a similar way, the signal generated

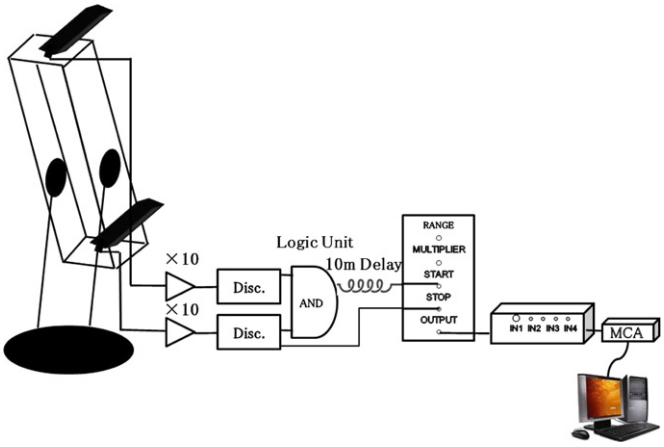

Figure 1. Scheme of the electronics layout used to record muon decay.

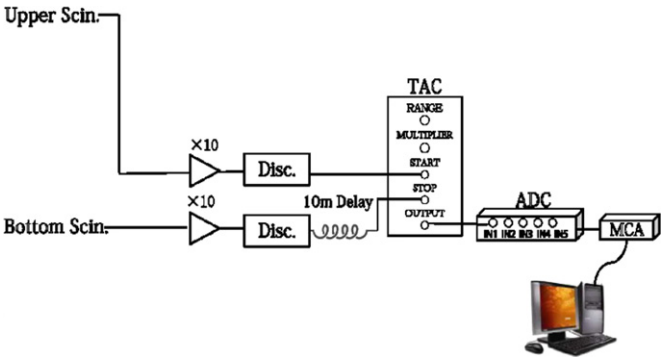

Figure 2. A schematic view of the electronics used to record coincidence events of the apparatus.

by the bottom PMT is directed to the 'stop' input of the TAC by a 10 m delay cable. Finally the output of the TAC is sent to the MCA via an ADC. The delay cables provide adjustable delays which permit a shortening or lengthening of the electronic paths in a coincidence circuit. A schematic view of the electronics used to record coincidence events of the apparatus is shown in figure 2.

3. Experimental measurements and data analysis

The total muon decay curve is a superposition of several decay laws as follows [2, 7]:

$$\frac{\mathrm{d}N}{\mathrm{d}t} = \frac{N_{\mu^+}}{\tau_{\mu^+}}\mathrm{e}^{\left(\frac{-(t+\tau_{\mathrm{delay}})}{\tau_+}\right)} + \frac{\mathrm{N}_{\mu^-}}{\tau_{\mu^-}}\mathrm{P}_{\mathrm{decay}}\mathrm{e}^{\left(\frac{-(t+\tau_{\mathrm{delay}})}{\tau_-}\right)} + \mathrm{C}_{\mathrm{bg}}\mathrm{e}^{\left(\frac{-(t+\tau_{\mathrm{delay}})}{\tau_{\mathrm{bg}}}\right)} + \epsilon_{\mathrm{bg}}, \tag{6}$$

where the first and second terms are related to positive and negative muon decay and the third and fourth terms are related to background radiation. P_{decay} represents the decay probability of negative muons in the scintillator; τ_{delay} indicates the delay time due to a lengthening in the electronic path for the signal of the stopped muon by the 10 m cable in the experimental circuit; τ_{bg} stands for the time constant of background radiation and ϵ_{bg} is a constant background. Decay experiments were operated in 168 h time intervals and repeated seven times. In all decay experiments, the telescope was positioned vertically.

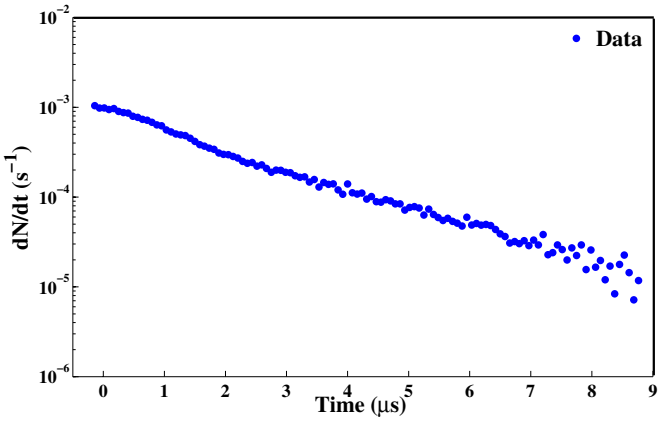

Figure 3. The experimental data decay curve after subtracting background.

Due to the probability of recording double-particle events by the electronic circuit which are considered as a background, we carried out a series of new experiments. In the double-particle events signals due to sources other than decay electrons, e.g. other incident muons (or some other charged particles), background events, noise in the bottom scintillator etc, would also trigger a stop signal in the TAC. In order to record these events with no limitation in the solid angle of detection (incoming particles from all zenithal angles) and other backgrounds together with events which are related to the muon decay, we used only one scintillator. In this way both the signals which trigger and halt the TAC are sent from one scintillator.

By analysing the recorded events and fitting equation (6) to the obtained data, the average time constant (τ_{bg}) was obtained as 284.8 ns. Finally by fitting equation (6) to muon decay experimental data which are recorded in 168 h (one week) time intervals, we determined the muon charge ratio. The average muon charge ratio together with its statistical uncertainty was obtained as 1.15 ± 0.03 in 168 h time intervals. The error in R_μ is that of the corresponding parameters in the fitting procedure. In figure 3 an example of the experimental data decay curve after subtracting background is shown.

To evaluate the systematic time-dependent effects of the muon charge ratio, we grouped experimental decay data together and made data in 336–1176 h (two to seven weeks) time intervals. The values of the muon charge ratio at different time intervals (figure 4) show that the fluctuations are very small and for a three-week time interval or more, the values of $\overline{R}_\mu$ tend to a fixed amount 1.18 ± 0.02. Figure 5 shows the muon charge ratio results obtained by different experimental techniques up to 10 GeV muon energy [7, 14, 15]. The filled circle shows our recent results ($R_\mu = 1.18 \pm 0.02$) in the momenta range 0.76–1.60 GeV/c. This momenta range is obtained by considering the minimum and maximum path of incident muons which pass through the top scintillator and stop in the bottom scintillator and by using the Bethe–Bloch formula in order to average the energy loss of the muons.

To study the muon angular distribution we measured muon flux at four cardinal directions of 0° (North), 90° (West), 180° (South) and 270° (East) and three zenith angles of $20° \pm 17°$, $40° \pm 17°$ and $60° \pm 17°$. The measurements were carried out in 24 h time intervals. Table 2 shows the muon flux in different directions.

Since the dependence of muon flux on zenith angle is as $I(\theta) = I(0)\cos^n\theta$ [16], we estimated n by fitting this function to experimental data. The values of n were obtained as $n = 1.90 \pm 0.16$, $n = 1.91 \pm 0.15$, $n = 1.90 \pm 0.14$ and $n = 1.92 \pm 0.27$ for the directions

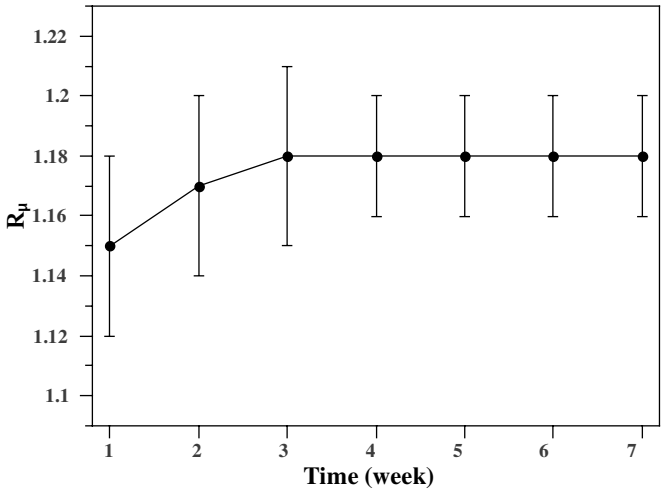

Figure 4. Determination of the muon charge ratio using data obtained at different time intervals.

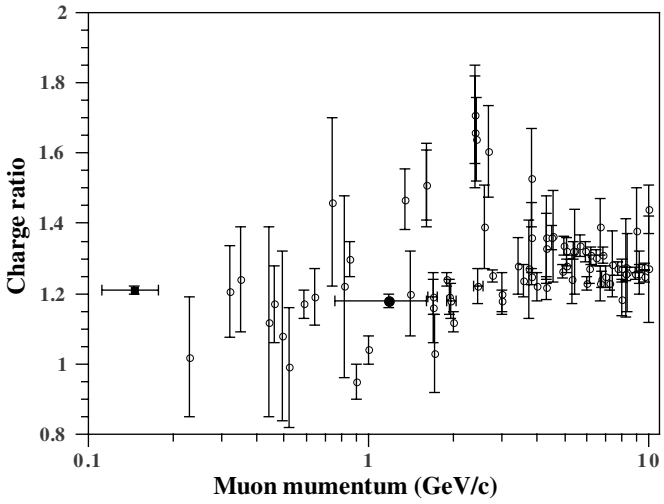

Figure 5. Compilation of the muon charge ratios up to 10 GeV/*c* muon momentum from different experiments [7, 14, 15]. (•) presents our recent result in the momentum range 0.76–1.60 GeV/*c* and (■) presents our previous result in the momentum range 0.112–0.178 GeV/*c* [11].

Table 2. Muon flux ($m^{-2}sr^{-1}s^{-1}$) obtained in different directions.

Azimuth angle	$\theta = 0^\circ$	$\theta = 20^\circ$	$\theta = 40^\circ$	$\theta = 60^\circ$
$\phi = 0^\circ$	219.28 ± 1.64	196.11 ± 1.56	128.32 ± 1.26	61.58 ± 0.87
$\phi = 90^\circ$	219.28 ± 1.64	195.27 ± 1.55	128.05 ± 1.26	61.24 ± 0.87
$\phi = 180^\circ$	219.28 ± 1.64	195.72 ± 1.55	128.47 ± 1.26	61.12 ± 0.87
$\phi = 270^\circ$	219.28 ± 1.64	186.09 ± 1.52	125.51 ± 1.24	60.65 ± 0.86

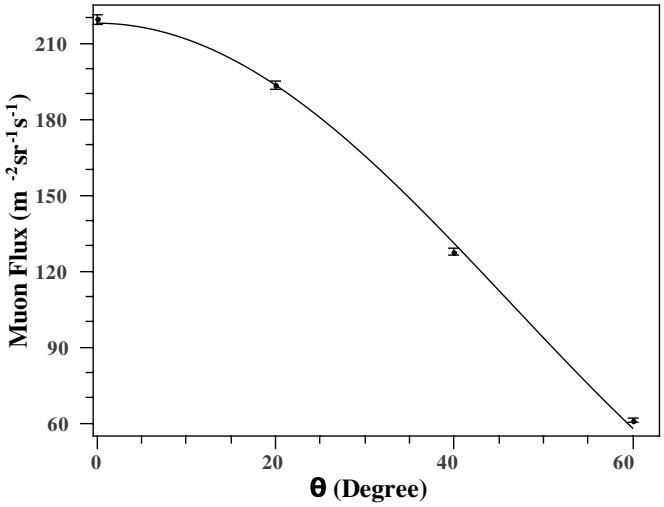

Figure 6. Average muon flux at different zenith angles.

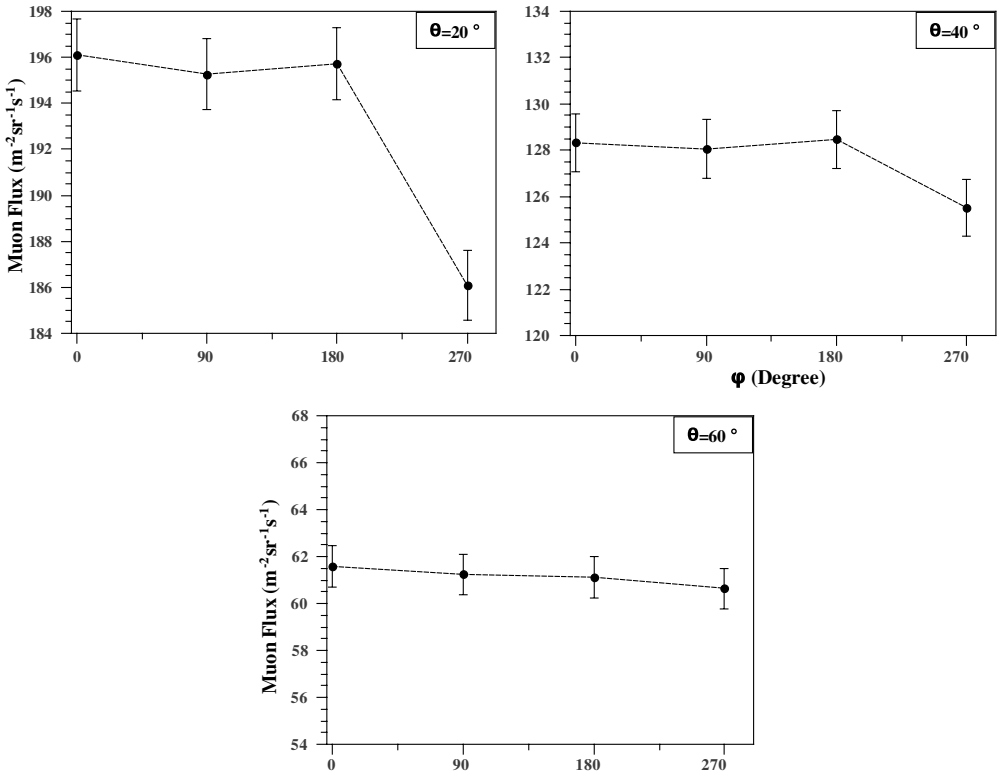

Figure 7. Average muon flux at different azimuth angles, for zenith angles $\theta = 20^\circ$, 40°, and 60°.

North, West, South and East respectively with regression more than 98%. In figure 6, the average muon flux integrated on all azimuth angles versus zenith angle is shown. The value $n = 1.91 \pm 0.07$ is obtained from this figure. In addition, figure 7 shows the comparison of

muon flux versus different azimuth angles for zenith angles $\theta = 20^\circ$, 40° and 60°. For $\theta = 20^\circ$ asymmetry in the West–East direction is obvious.

4. Monte Carlo simulations

The motivation to simulate air showers initiated by protons and alpha particles as the most probable of all possible primary particles is to compare those simulated showers with measurements and to test different hadronic interaction models.

For the air shower simulations the program CORSIKA (version 6.9) has been used with different hadronic interaction models. UrQMD [17] and GHEISHA [18] models (E $\leqslant$ 100 GeV and 80 GeV, respectively) have been used for hadronic interactions at low energy and for high-energy interactions, the QGSJET-II [19] model is used. In the performed simulations, primary particles (proton and alpha) inducing EASs are considered with an incidence zenith angle of $\theta \leqslant 60^\circ$ and arriving from different cardinal directions: North, West, South and East. The energy range for primary particles was selected as 10^{11}–10^{16} eV because below 100 GeV the contribution of primary particles (proton and helium) to the intensity of muons which are detectable by the apparatus is negligible. The Earth's magnetic field ($B_x = 27.99\ \mu$T, $B_Z = 38.49\ \mu$T), the observation level (1200 m a.s.l.), the secondary muon momenta range (0.76–1.60 GeV/c) and zenith angles of them ($\theta \leqslant 17^\circ$) have been chosen according to the conditions of the experiments. Approximately 2600 showers have been simulated. For each shower the muon charge ratio has been obtained.

Finally, the muon charge ratio was obtained as 1.08 ± 0.07 with the QGSJET–GHEISHA models and as 1.16 ± 0.08 with the QGSJET–UrQMD models. It can be seen that the predictions of the QGSJET–UrQMD models are more compatible with our experimental result.

5. Concluding remarks

The muon charge ratio was determined by using a cosmic ray telescope at SUT in Tehran at 1200 m a.s.l (890 g cm^{-2}). The momenta range of detectable muons by the telescope (0.76–1.60 GeV/c) was estimated according to the energy loss of travelling muons through the scintillators which is described by the Bethe–Bloch formula. Due to recorded events which are related to double-particles and are considered as noise, a series of experiments were performed and the time constant of background radiation, τ_{bg}, was obtained as 284.8 ns by means of exponential fits (equation (6)) to these data. Finally the muon charge ratio was obtained as 1.15 ± 0.03 in a 168 h time interval. Also obtained were values for the muon charge ratio at different time intervals which show that fluctuations are very small and for the 504 h time interval or more, $\overline{R}_\mu$ tends to a fixed value of 1.18 ± 0.02.

To study the muon component in more detail, Monte Carlo simulations of EASs with CORSIKA code have been performed with respect to existing experimental conditions. Finally by selecting muons in the allowed momenta range (0.76–1.60 GeV/c), the muon charge ratio was obtained sd 1.08 ± 0.07 and 1.16 ± 0.08 by the QGSJET–GHEISHA and QGSJET–UrQMD models respectively.

The muon angular distribution shows an asymmetry in received flux from West to East due to the influence of magnetic field especially for low energy particles. In addition, dependence of muon flux on zenith angle was obtained as $I(\theta) = I(0)\cos^n\theta$ with $n = 1.90 \pm 0.16$, $n = 1.91 \pm 0.15$, $n = 1.90 \pm 0.14$ and $n = 1.92 \pm 0.27$ for the cardinal directions North, West, South and East respectively. Finally the value $n = 1.91 \pm 0.07$ was obtained from integration on all azimuth angles.

Acknowledgments

We thank S Mortazavi Moghaddam for substantial help in operating the apparatus. We acknowledge the anonymous referees for their constructive comments.

References

[1] Wentz J *et al* 2001 *J. Phys. G: Nucl. Part. Phys.* **27** 1699
[2] Vulpescu B *et al* 2001 *J. Phys. G: Nucl. Part. Phys.* **27** 977
[3] Hebbeker T and Timmermans C 2002 *Astropart. Phys.* **18** 107
[4] Gaisser T K and Stanev T 1998 *Phys. Rev.* D **38** 85
[5] Honda M *et al* 1995 *Phys. Rev.* D **52** 4985
[6] Fukuda Y *et al* 1998 *Phys. Lett.* B **436** 33
Fukuda Y *et al* 1998 *Phys. Rev. Lett.* **81** 1562–7
[7] Vulpescu B *et al* 1998 *Nucl. Instrum. Methods* A **414** 205
[8] Tsuji S *et al* 1998 *J. Phys. G: Nucl. Part. Phys.* **24** 1805
[9] Heck D *et al* 1998 *Report* FZKA 6019 Forschungszentrum Karlsruhe
[10] Bahmanabadi M, Khakian Ghomi M and Sheidaei F 2005 *Astropart. Phys.* **24** 183–90
[11] Bahmanabadi M, Sheidaei F, Khakian Ghomi M and Samimi J 2006 *Phys. Rev.* D **74** 082006
[12] Wheeler J A 1949 *Rev. Mod. Phys.* **21** 133
[13] Suzuki T, Measday D F and Roalsvig J P 1987 *Phys. Rev.* C **35** 2212
[14] Khachatryan V *et al* (CMS Collaboration) 2010 *Phys. Lett.* B **692** 83–104
[15] Haino S *et al* 2004 *Phys. Lett.* B **594** 35–46
[16] Grieder P K F 2001 *Cosmic Rays at Earth (Researcher's Reference Manual and Data Book)* (Amsterdam: Elsevier) p 25
[17] Bass S A *et al* 1998 *Prog. Part. Nucl. Phys.* **41** 255
Bleicher M *et al* 1999 *J. Phys. G: Nucl. Part. Phys.* **25** 1859
[18] Fesefeldt H 1985 *RWTH Aachen Report No.* PITHA85/02
[19] Kalmykov N N *et al* 1997 *Nucl. Phys.* B **52** 17